Agronomy Research **23**(2), 1185–1202, 2025
https://doi.org/10.15159/AR.25.060

Assessment of the spatiotemporal changes of saline-alkaline soils using GIS and, geospatial technologies methods: a community case study

A.O. Markosyan[1], M.H. Zadayan[2,*], G. Azgaldyan[3], S.K. Baghdasaryan[1], S.Z. Kroyan[4] and S.A. Markosyan[5]

[1]Armenian National Agrarian University, Scientific Center of Soil Science, Agrochemistry and Melioration named after H. Petrosyan, Department of Soil Science, Agrochemistry and Geography of Soils, 24 Admiral Isakov Ave, AM0004 Yerevan, Armenia
[2]Center for Agricultural Research and Certification, State Non-Commercial Organization of the Ministry of Economy of the Republic of Armenia, Yerevanyan highway 2nd deadlock, building 4, Armavir Marz, v. Merdzavan, AM1139, Armenia
[3]Hydrometeorology and Monitoring Center of the Ministry of Environment of the Republic of Armenia, State Non-Commercial Organization, GIS and Remote Sensing Service, 46 Charenc, AM0025 Yerevan, Armenia
[4]National University of Architecture and Construction of Armenia, Department of Engineering Geodesy, Teryan St. 105, AM0009, Yerevan, Armenia
[5]Yerevan State University, Faculty of Biology, Department of Biology, 1 Alex Manoogian, AM0025 Yerevan, Armenia
[*]Correspondence: mhzadayan@gmail.com

Received: March 13th, 2025; Accepted: June 19th, 2025; Published: July 3rd, 2025

Abstract. Currently, in many countries, soil salinization is recognized as one of the primary land degradation processes, particularly in arid regions, where it significantly limits soil fertility and worsens ecological conditions.
The widespread occurrence of solonetzic soils, including soda-type saline-alkaline soils, along with the intensification of salinization under changing climatic conditions and anthropogenic pressure, highlights the urgent need to update data on their distribution and expansion trends.
This study, conducted between 2020 and 2022, presents the results of a survey of 600 hectares of saline soils in the Mrgashat settlement, Armavir Region, Republic of Armenia (center coordinates: 44° 5′ 14.36″ E, 40° 7′ 14.57″ N). A quantitative and qualitative assessment of the current state was carried out using GIS and remote sensing data, alongside soil sampling from six designated points.
Newly salinized areas over the past 10 years were mapped, and the dynamics and direction of salinization were analyzed. The validity of the findings was corroborated by field survey data and relevant statistical indicators.
The results indicate a clear trend of spatial and temporal expansion of salinized soils. Over the last two decades, the total salinized area has increased by 54 hectares, representing a 10.1% growth.

Key words: satellite imagery, vegetation indices, soil salinity, salinity mapping, spectral analysis, salinity index, remote sensing.

INTRODUCTION

Salinity is a spatiotemporally dynamic process of land degradation in semi-arid regions that reduces both the productivity and extent of agricultural land (Periasamy & Ravi, 2020; Xiang et al., 2022). Although the salinization of drylands poses a significant threat to land and water resources in many countries, its importance has only recently gained broader recognition (FAO, 2005).

According to the Food and Agriculture Organization of the United Nations (FAO), the total global area of saline soils amounts to 397 million hectares (FAO, 2005). These soils are prevalent in Africa, Asia, Australia, Europe, Latin America, the Middle East, and North America (Koohafkan & Stewart, 2008; Tong et al., 2023; Calderon Pincay & Pincay Cantos, 2024). For instance, McFarlane et al. (2004) estimated that in Western Australia alone, 14,000 hectares of land have been annually affected by secondary salinization since 1996, and approximately 3.54 million hectares are currently at risk – potentially doubling to 6.5 million hectares (33%) by 2050.

The Republic of Armenia is no exception. Various studies report that 40–45% of the Ararat Plain (about 40,000 ha) has been withdrawn from agricultural use due to varying degrees of salinization and alkalization (Khojoyan, 2013; Yeghiazaryan, 2017).

Salinization is a gradual and often imperceptible process. By the time visible signs emerge, substantial salt accumulation may have already occurred in the soil's active layer, impairing plant growth and development (Melkonyan et al., 2004). Therefore, early-stage monitoring and mapping of salinized areas and severity levels are critical for effective land management and mitigation (Koohafkan & Stewart, 2008; Yeghiazaryan & Yeghiazaryan, 2018).

Traditional salinity assessment methods are often time-consuming, labor-intensive, and costly. Consequently, the application of remote sensing (RS) techniques has become increasingly recommended (Yeghiazaryan, 2017; Smanov et al., 2023).

Modern satellite platforms offer diverse spectral and spatial datasets that support vegetation monitoring, climate assessments, and modeling of future scenarios (Abreu et al., 2024). These technologies allow efficient detection, mapping, and monitoring of salinization with acceptable accuracy (Dwivedi et al., 2008; Zhang et al., 2021).

However, RS accuracy peaks (approximately 83%) when visible surface salt deposits are present (Howari, 2003). In areas where halophytes are dominant or visible salt is absent, detection accuracy decreases (Howari et al., 2002; Shoba et al., 2016). In such cases, integrating satellite imagery with field survey data enhances reliability (Douaoui et al., 2006; Eldeiry & Garcia, 2008). For example, a study in Thailand using Landsat-7 ETM+ in combination with topographic and groundwater data achieved an overall mapping accuracy of 83.6% (Katawatin & Kotrapat, 2005).

In addition to visible and infrared bands, satellites such as Landsat 8 and 9 provide surface temperature and humidity data, which are essential for interpreting solonetzic soils (Baldina & Nikolaev, 2024). These thermal indicators are particularly useful in identifying saline soils in bare or sparsely vegetated regions (Koohafkan & Stewart, 2008).

Nevertheless, medium or low spatial resolution can limit RS accuracy when affected zones are smaller than one pixel. Therefore, high-resolution multispectral sensors (< 5 m) are critical for detecting small-scale salinization (Dwivedi et al., 2008).

Although satellite technology is rapidly advancing, historical data remains crucial for long-term land degradation modeling (Burke et al., 2021). Vegetation indices provide valuable insights into both soil salinity and its effects on crop productivity (Wang et al., 2021; Silva, 2024). Halophytic vegetation, in particular, serves as a reliable remote indicator for salinity detection and mapping (Koohafkan & Stewart, 2008; FAO Guidelines, 2017).

Certain salt-tolerant crops, such as alfalfa, barley, and cotton, are also used as indirect indicators of soil salinity in research (Metternicht & Zinck, 2008).

Numerous spectral indices have been employed to classify and monitor salinized land, including NDVI, SAVI, RVI, Tasseled Cap Transformation, SBI, GVI, WI, NDSI, and various salinity indices (Eldeiry & Garcia, 2008; Matinfar et al., 2013; Nguyen et al., 2020). Each is suitable for specific land cover types and salinity conditions. For example, NDVI effectively maps halophyte presence (Elnaggar & Noller, 2009), while SAVI has been applied in the UAE for salinity detection via plant vigor analysis (Huete, 1988; Alhammadi & Glenn, 2008). NDSI helps distinguish saline from non-saline soils based on spectral differences (Nguyen et al., 2020).

Despite extensive international research, no unified methodology for monitoring soil salinity using GIS and RS currently exists. In Armenia, earlier studies have been limited in scale and lack practical application for broad salinity assessments.

Therefore, the aim of this study was to evaluate the effectiveness of combining GIS, remote sensing methods, and field-based soil sampling for assessing the distribution and spatiotemporal dynamics of saline-alkaline soils. These assessments are crucial for designing sustainable management strategies, promoting crop diversification, and developing preventive measures to mitigate salinization.

MATERIALS AND METHODS

Study area

The research was conducted on saline-alkaline soils across a 600-hectare area within the Mrgashat settlement, Armavir Region, Republic of Armenia (Fig. 10. Sentinel-2 classification map showing reclaimed lands).

The soil profile is distinctly stratified and lacks the gradual transitions of genetic horizons typically found in soils developed on alluvial deposits (Hayrapetyan, 2000).

These soils are characterized by high salinity (total salt content: 1–3%), substantial carbonate content (15–20%), low humus levels (0.4–0.6%), and high alkalinity (pH 9–11). The soils also exhibit high exchangeable sodium concentrations (25–30 mEq per 100 g of soil, accounting for 60–80% of total exchangeable cations), and a medium to heavy loamy to clayey texture. Their hydrophysical properties are generally poor (Khojoyan, 2013).

The climate in the study area is classified as sharply arid, with hot, dry summers and snowy winters. The average annual air temperature ranges between 11.0 and 12.3 °C. Precipitation averages 200–235 mm annually, whereas evaporation is significantly higher, ranging from 1,160 to 1,480 mm (Hayrapetyan, 2000).

Remote sensing and GIS analysis

To evaluate the effectiveness of remote sensing (RS) and geographic information systems (GIS) for mapping saline soils, Landsat 8 satellite images were utilized in conjunction with salinity and vegetation indices, including the Normalized Difference Salinity Index (NDSI) and Normalized Difference Vegetation Index (NDVI). These datasets were processed using the ArcMap module of the ArcGIS software package. Field data collection and laboratory analysis were carried out to verify and enhance the reliability of the remote sensing results.

Software and image processing

The study employed both remote sensing and ground-truthing techniques to perform qualitative and quantitative assessments of saline soil distribution. A time-series analysis of satellite images was used to track salinity dynamics over a 20-year interval. Image classification was performed using both automated, computer-assisted techniques and visual interpretation. Input datasets included multi-temporal satellite imagery, scientific and thematic literature, statistical data, and official government sources. The following software platforms were used: ArcGIS 10.5, ENVI 5.3, and SNAP.

Satellite image acquisition and preprocessing

Satellite imagery was retrieved from the Land Viewer platform (EOS). Image selection was based on the following criteria:

- Cloud-free conditions
- Seasonal consistency (summer)
- A 20-year time interval
- Availability of complete pixel information.

Based on visual inspection and data quality, the following images were selected for analysis:

- Landsat 7 (acquired on 13 August 2000)
- Landsat 8 (acquired on 20 August 2020).

The selected images underwent geometric and radiometric correction using ENVI 5.3. FLASH atmospheric correction was applied as part of the preprocessing workflow.

Summer-season imagery was prioritized due to enhanced spectral contrast between salt deposits and halophytic vegetation, which is particularly pronounced during the dry season.

Salinity and vegetation indices

Saline landscapes are typically characterized by sparse or stressed vegetation. Therefore, specific spectral indices were used to identify and map salt-affected soils (Table 1). These include:

- Brightness Index (BI)
- Normalized Difference Salinity Index (NDSI)
- Salinity Indices (SI1, SI2, SI3, SI4, SI5)
- Normalized Difference Vegetation Index (NDVI)
- Normalized Difference Moisture Index (NDMI).

Table 1. Various spectral indices and class formulas were used in the present study

Index	Formula	Reference
NDVI	(NIR - R) / (NIR + R)	Tucker, 1979
NDMI	(NIR - SWIR) / (NIR + SWIR)	Gao, 1996; Wilson & Sader, 2002
NDWI	(Green - NIR) / (Green + NIR)	Gao, 1996; McFeeters, 1996
NDSI	(R - NIR) / (R + NIR)	Khan et al., 2005
BI	$\sqrt{(R^2 + NIR^2)}$	Khan et al., 2005
SI1	$\sqrt{(B \times R)}$	Douaoui et al., 2006
SI2	$\sqrt{(G^2 + R^2 + NIR^2)}$	Douaoui et al., 2006
SI3	$(SWIR1 \cdot SWIR2 - SWIR2^2) / SWIR1$	Bannari et al., 2008
SI4	$(R \cdot NIR) / G$	Abbas & Khan, 2007
SI5	$(G \cdot R) / B$	Bannari et al., 2008

Note: B = Blue; G = Green; R = Red; NIR = Near-Infrared; SWIR1, SWIR2 = Shortwave Infrared bands.

Field sampling and soil analysis

While remote sensing provides valuable information for identifying salt-affected areas, field validation is essential for ensuring accuracy and model calibration.

Based on the interpretation of satellite images, the most salt-affected zones were identified in the eastern part of the Mrgashat settlement. This zone, covering approximately600 hectares, was selected for detailed investigation.

Soil samples were collected from the topsoil layer (0–40 cm) at six representative points. The GPS coordinates of each sampling location were recorded using a handheld positioning device with a spatial resolution of 1.5 meters (Table 2).

Table 2. Soil sampling locations and coordinates

No	Sampling site	Longitude (E)	Latitude (N)
1	Train line	44° 5′ 28.235″	40° 7′ 46.709″
2	Cultivated field	44° 5′ 51.633″	40° 7′ 30.714″
3	Saline-cultivated field	44° 4′ 46.094″	40° 7′ 12.730″
4	Halophyte area	44° 5′ 28.194″	40° 7′ 6.815″
5	Severely saline zone	44° 4′ 51.296″	40° 6′ 55.230″
6	Salt crust zone	44° 5′ 32.057″	40° 7′ 21.439″

To align the field data with satellite imagery (on a pixel-based scale), soil samples were collected directly from visible salt crusts identified through remote sensing. Pixels with similar spectral characteristics were grouped, and pseudo-sampling points were introduced to enhance representativeness and improve the reliability of interpolation results.

Five key indicators derived from laboratory analysis were selected for interpolation:

- pH
- Sodium (Na)
- Magnesium (Mg)
- Calcium (Ca)
- Salinity (total dissolved salts in aqueous extract).

Laboratory analyses were performed at the Hydrometeorology and Monitoring Center SNCO using standard methods and advanced instrumentation, including:

- X-ray fluorescence (XRF)
- Inductively coupled plasma mass spectrometry (ICP-MS)
- Ion chromatography (IC).

The results are summarized in Tables 3–6.

RESULTS AND DISCUSSION

Remote sensing indicators and image interpretation

Experimental results demonstrated that no individual spectral index alone provided a complete and accurate representation of soil salinity. Reliance on a single indicator often resulted in substantial misinterpretations and classification errors (Fig. 1).

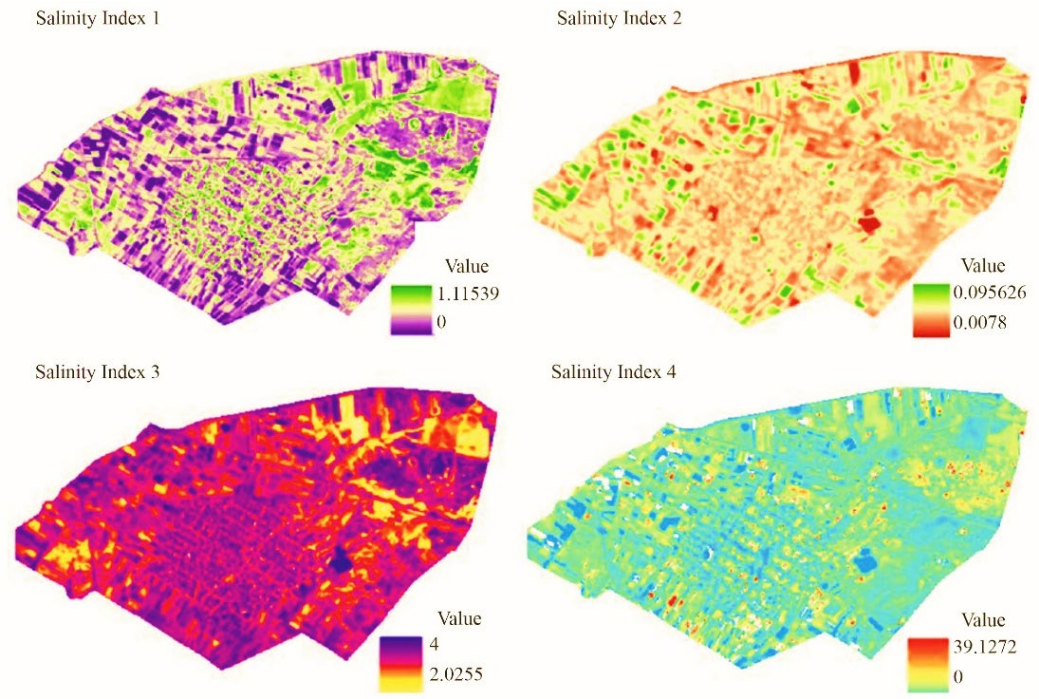

Figure 1. Soil salinity classification in the Mrgashat area based on individual salinity indices.

Given that certain areas were covered with halophytic vegetation, several vegetation indices were also evaluated alongside the salinity indices to enhance classification accuracy (Fig. 2).

Among the indices evaluated, the Normalized Difference Salinity Index (NDSI) most accurately represented actual salinity conditions observed during field validation. However, certain factors reduced detection accuracy:

- Metal roofs and other reflective surfaces produced spectral signatures similar to salt crusts, leading to false positives
- Bare or recently ploughed fields also exhibited high reflectance values, mimicking saline features due to their brightness.

Integration of auxiliary indices

To enhance mapping precision, two additional spectral indicators were integrated into the analysis:

- Land Surface Temperature (LST)
- Normalized Difference Moisture Index (NDMI).

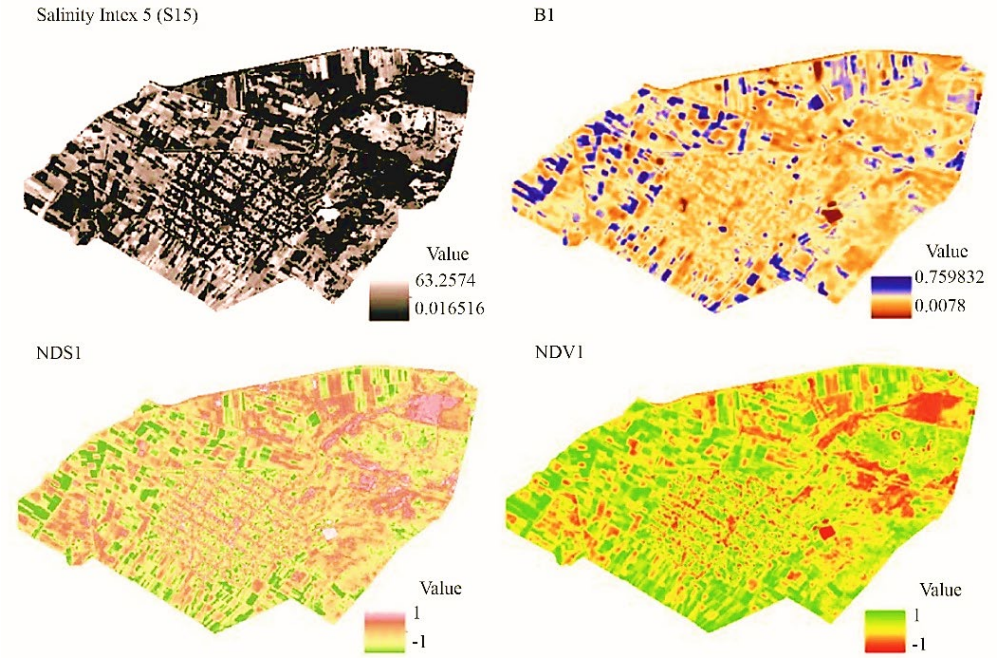

Figure 2. Soil salinity and vegetation classification of the Mrgashat area based on spectral indicators.

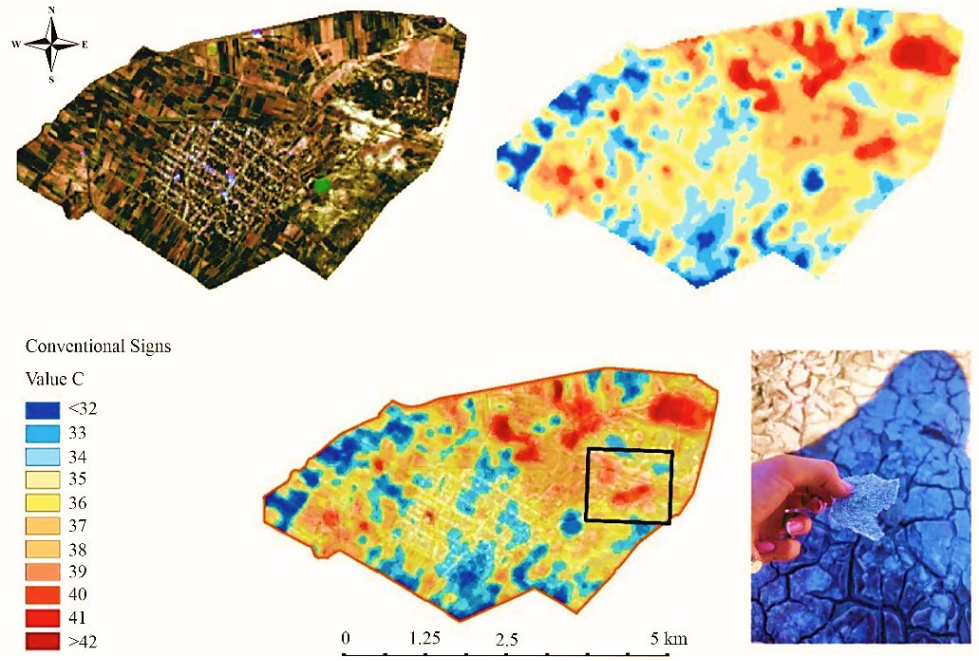

Figure 3. LST raster image of the Mrgashat area (Landsat 8, 28 August 2020).

LST values were derived from the thermal bands of Landsat 8 (acquired on August 28, 2020) using ENVI 5.3, and subsequently calibrated to degrees Celsius (Fig. 3). Surface temperatures in the study area ranged between 32 °C and 42 °C, and were classified into 11 discrete levels.

The Normalized Difference Moisture Index (NDMI) integrates near-infrared (NIR) and shortwave infrared (SWIR) bands to serve as an effective indicator of crop water stress. Severe drought conditions can not only stress crops but also lead to complete crop failure. NDMI is particularly valuable for early detection of water stress, often identifying problems before they become visually apparent.

Our analysis indicates that moisture levels near the boundaries of saline surfaces offer useful contrast. These levels help distinguish saline soils from non-saline reflective surfaces such as rooftops, which exhibit low moisture and appear as hotspots in the LST raster due to their elevated surface temperatures (Fig. 4).

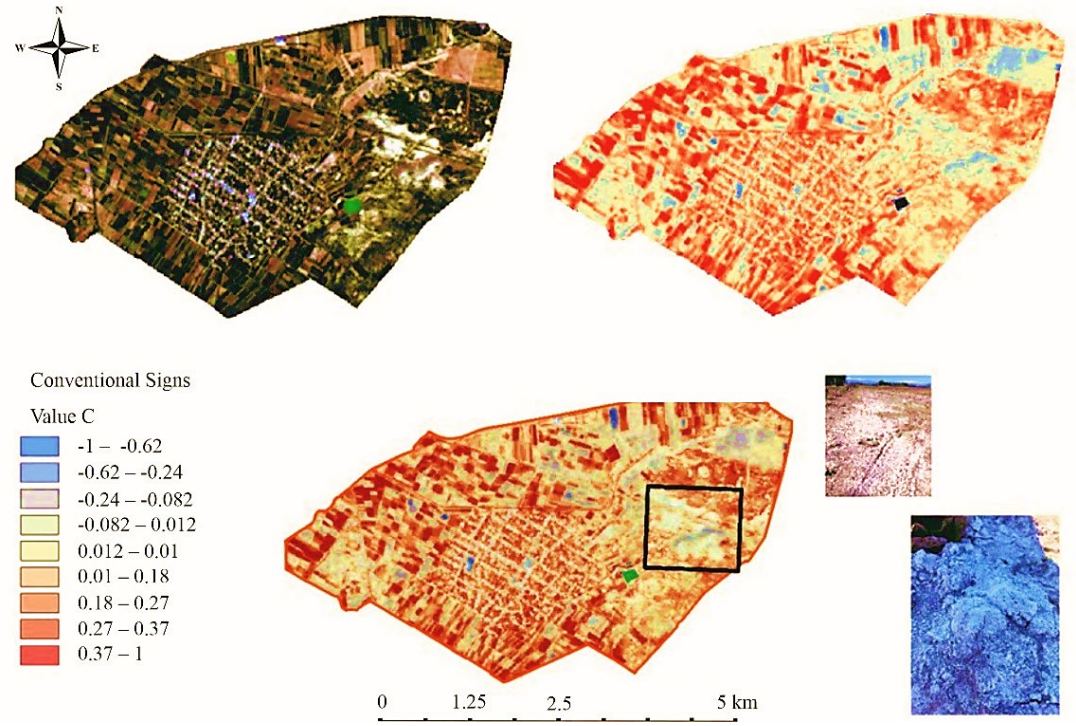

Figure 4. NDMI image of the Mrgashat area (Landsat 8, 28 August 2020).

To enhance classification accuracy, five key indices were integrated into composite raster layers:

- NDVI – Vegetation health
- NDSI – Soil salinity
- NDMI – Surface moisture
- BI – Brightness Index
- LST – Land surface temperature.

Each of these indices provided a distinct representation of salt-affected zones and their surrounding areas. To obtain the most accurate classification, various combinations of these indices were tested, resulting in new composite raster datasets. The spectral components of these composites were derived from the previously calculated indices: NDVI, NDSI, NDMI, BI (Khan et al., 2005), and LST (Fig. 5).

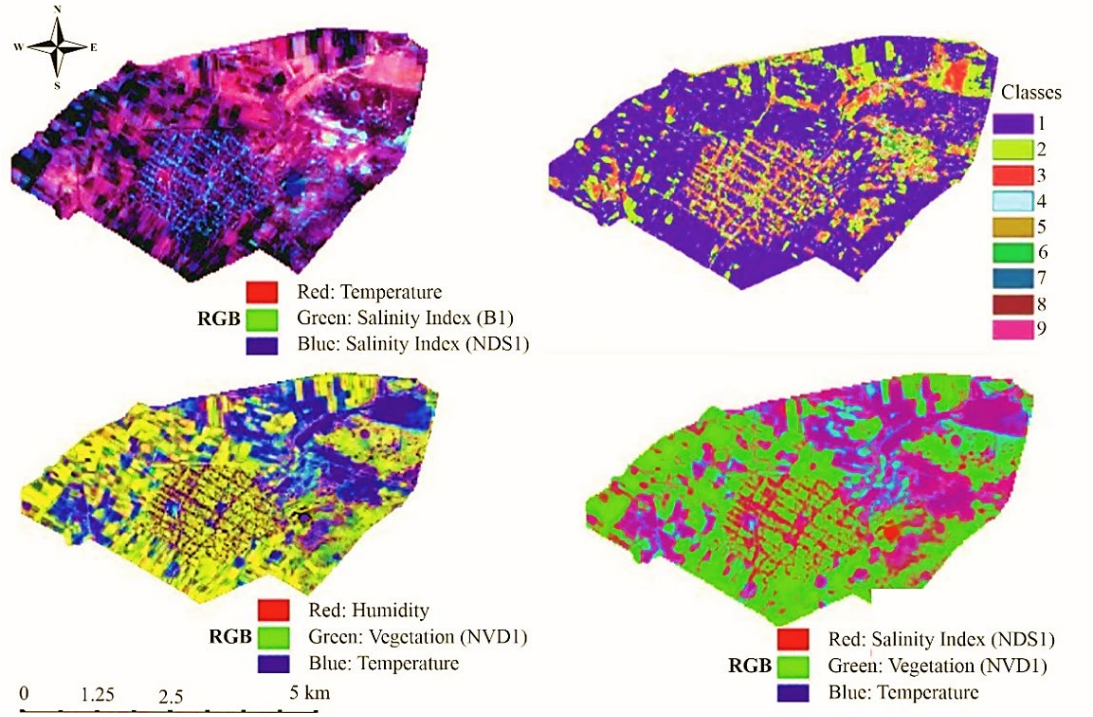

Figure 5. Composite image of Mrgashat lands based on integrated spectral indices.

Classification and Salinity Mapping

Using the Normalized Difference Salinity Index (NDSI) along with the previously derived raster datasets, pixel-based classification was performed. Classification intervals were determined based on the statistical distribution of pixel values for each index.

To validate and refine classification accuracy, vector layers of saline areas - recorded with GPS during field visits (2020–2022) - were overlaid. The *Raster to Polygon* tool in ArcGIS was used to convert classified raster layers into vector shapefiles.

Composite overlays and cross-validation among indices minimized false positives and improved salinity detection accuracy:

- BI (Brightness Index): Identified areas with strong reflectance, primarily surface salt crusts. Filtered using NDMI to exclude high-reflectance non-saline features (e.g., rooftops)
- NDVI: Mapped halophytic vegetation; filtered using LST (Land Surface Temperature) to exclude thermal anomalies
- NDSI: Highlighted areas with minimal visible salt deposits; further refined through combination with other indices.

These filtering steps allowed for precise delineation of actual saline areas from built-up or vegetated land. Final salinity maps were developed for the years 2000 and 2020, classifying affected land into three severity levels (Fig. 6):

1. Severely saline: Surfaces with visible salt crust accumulation.
2. Moderately saline: Transitional areas between crusted zones and vegetated regions.
3. Halophytic vegetation zones: Dominated by salt-tolerant plant species.

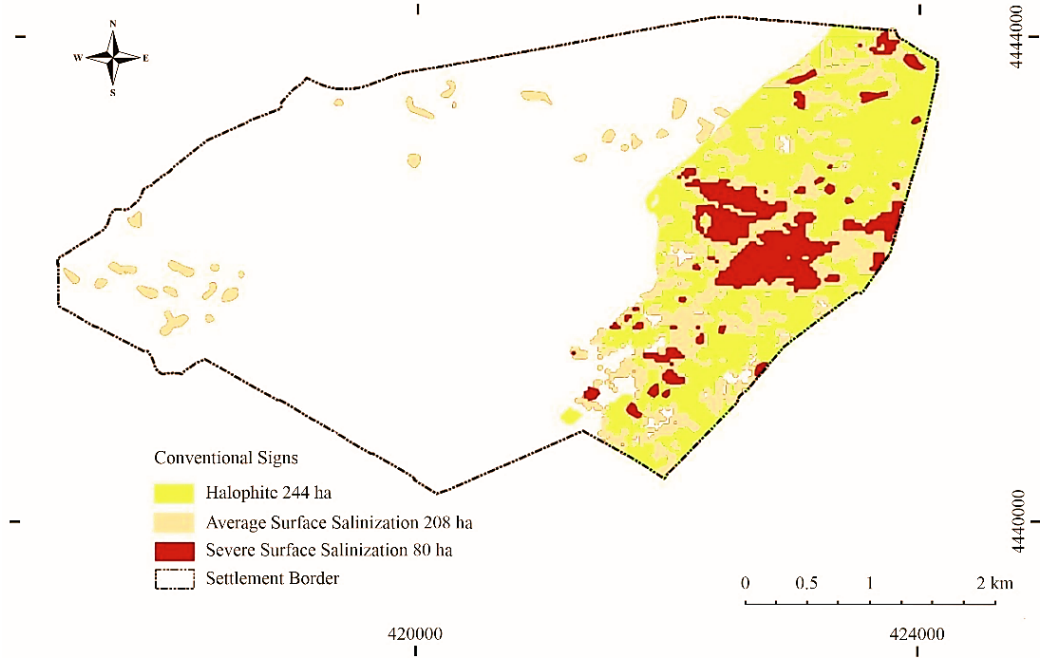

Figure 6. Map of salinity classification in Mrgashat (2000 satellite image).

The total salinized area in 2000 was estimated at 532 hectares, with the following classification:

- Halophytes: 244 ha
- Moderately saline: 208 ha
- Severely saline: 80 ha.

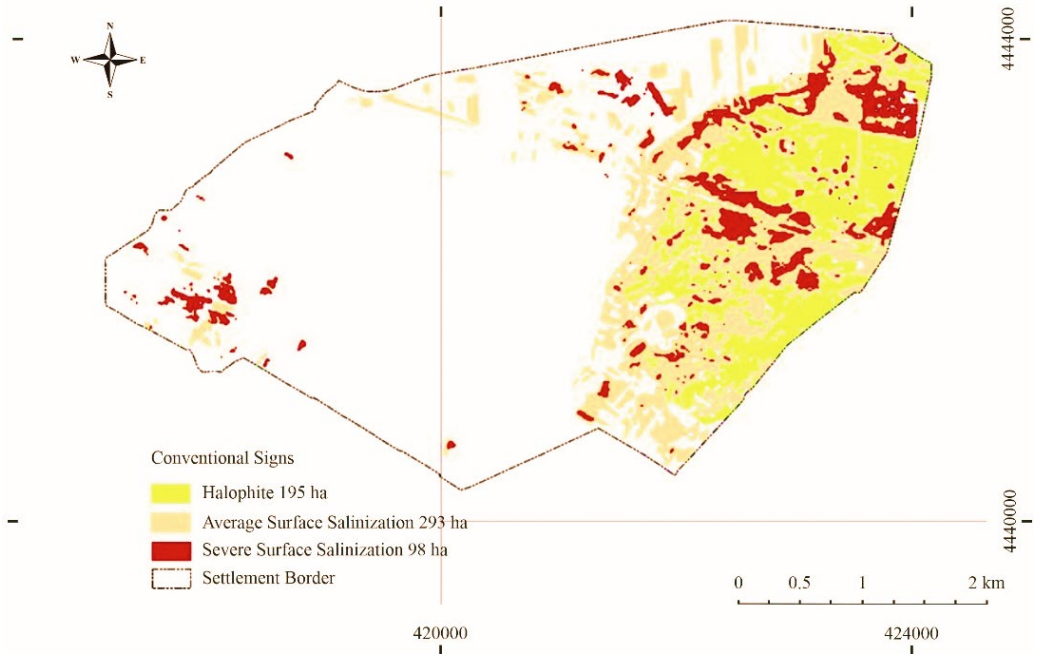

Figure 7. Salinity classification map of Mrgashat (2020 satellite image).

In 2020, the total affected area increased to 586 hectares (Fig. 7), with the following distribution:

- Halophytes: 195 ha
- Moderately saline: 293 ha
- Severely saline: 98 ha.

The net increase in salinized area was 54 hectares between 2000 and 2020. While some inaccuracies are possible - primarily due to the lower spatial resolution (30 meters) of the 2000 satellite imagery - overall trends remain consistent and reliable. Despite the limitations of the imagery, notable changes were detected across salinity classes.

Time-series image analysis revealed the following trends:

- Reduction in halophytic vegetation in areas subjected to plowing and cultivation
- Emergence of surface salt accumulations in nearby uncultivated areas over time.

These findings underscore the dynamic interplay between land use practices and salinization patterns (Fig. 8).

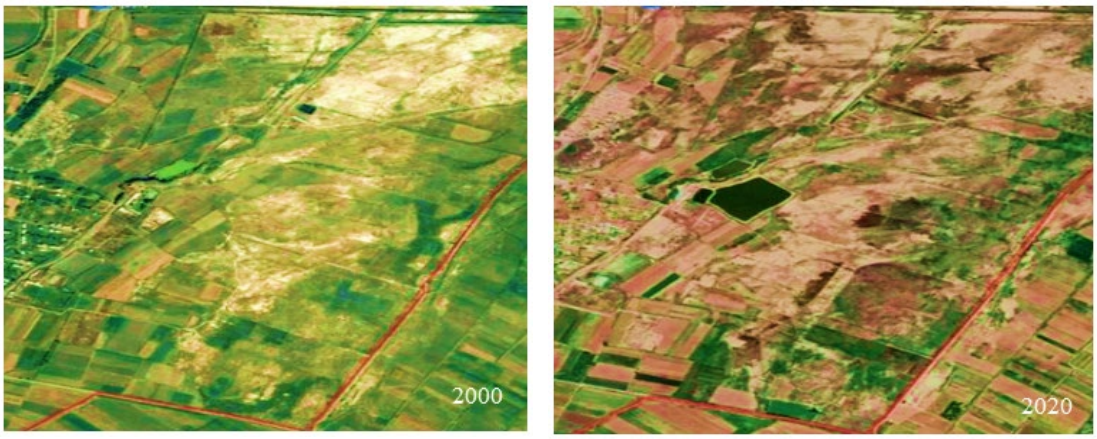

Figure 8. Changes in salinized surfaces due to land-use alterations.

This figure was derived by comparing the classified salinity layers from 2000 and 2020 with the current land surface temperature (LST) raster. The comparison highlights spatial dynamics in salinization patterns related to land-use changes over the past two decades.

Table 3 summarizes soil surface temperatures (in °C) across the classified salinity zones, based on satellite-derived thermal bands. These data provide additional insight into the correlation between surface temperature and salinity severity, supporting the identification of active versus passive salinization processes.

Table 3. Soil surface temperature (°C) based on satellite thermal bands

Class	2000			2020		
	Min	Max	Average	Min	Max	Average
Halophyte	33.8	46.9	39.7	29.2	40.4	35.2
Medium	33.3	49.3	42.5	33.3	42.2	36.8
Severe	35.2	46.9	44.2	32.2	41.7	38.2

The lowest temperatures consistently corresponded to halophyte-covered areas.

Soil sampling results and land use comparison

Field investigations confirmed significant soil salinization in the study area, as shown in Table 4. The following ranges were observed:

- Electrical conductivity (EC): 18.18–67.68 mS cm^{-1}
- Soluble salt content: 8.2–36.4 g L^{-1}
- pH: 9.57–10.39.

Table 4. Soil Electrical Conductivity (EC) and salt content (field and aqueous extract measurements)

N	pH	Directly in the soil		In the water column	
		EC (soil) mS	Salt (soil) g kg^{-1}	EC (solution) mS	Salt (solution) g kg^{-1}
1	9.57	12.07	> 2.99	27.24	12.72
2	10.07	5.33	1.91	18.18	8.2
3	10.07	5.33	1.91	18.18	8.2
4	9.58	21.73	> 2.99	35.42	16.8
5	10.37	7.34	2.6	21.44	9.8
6	10.09	24.69	> 2.99	67.68	36.4

These measurements indicate that the soils are strongly to very strongly saline, which significantly impairs plant growth and agricultural productivity. The high alkalinity (pH above 9.5) further exacerbates limitations for crop development.The dominant salts in the soil include sodium, magnesium, and calcium sulfates, chlorides, carbonates, and bicarbonates. Among them, sodium bicarbonate has the most toxic and detrimental effect on plant health, followed by sodium chloride.

Ionic composition analysis (IC) revealed high concentrations of SO_4^{2-} (2.3–10.0 mg kg^{-1}) and Cl^- (1.3–3.2 mg kg^{-1}). These two ions alone accounted for approximately 93.6% of total anions, a chemical environment that is unfavorable for crop development (Table 5).

Table 5. Ion chromatography (IC) results – anions (mg kg^{-1})

N	F	Cl^-	Br^-	NO_3^-	SO_4^{2-}	PO_4^{3-}
1	0.063	1.393	< 0.03	0.196	5.806	0.212
2	0.062	1.321	< 0.03	0.167	2.354	0.101
3	0.063	3.222	< 0.03	0.082	5.748	0.197
4	0.063	1.727	< 0.03	0.110	2.799	0.063
5	0.062	2.012	< 0.03	0.174	4.477	0.128
6	0.083	3.036	< 0.03	0.294	9.890	0.157

XRF and ICP-MS analyses revealed significant variations in macroelement concentrations and elevated levels of soluble salts across the study area.

The qualitative composition of salts influences soil appearance and behavior. In soils with high sodium bicarbonate concentrations, organic matter solubility increases, often giving the soil a darker color. Such characteristics were observed in certain locations within the study area.

A key diagnostic trait of saline soils is the uniform distribution of silt-sized particles – notably silicon, iron, and aluminum oxides – throughout the soil profile. Despite visual uniformity, saline soils are typically low in organic matter, nitrogen, and essential mineral nutrients.

Overall, the soils examined were highly saline, heterogeneous, and spatially variable, as detailed in Tables 6 and 7.

Table 6. XRF results – major elements (mg kg^{-1})

N	Al	Si	P	S	Cl	K	Ca	Fe
1	25,140	58,250	< 50	2053	1479	9,248	51,047	39,740
2	27,898	73,404	< 50	1153	1333	8,733	51,942	42,896
3	34,075	10,8957	< 50	3800	5692	10,051	53,920	41,368
4	24,425	56,222	< 50	1269	2756	7,751	49,693	39,724
5	26,719	64,847	< 50	1982	2867	7,837	49,356	39,916
6	25,070	67,269	< 50	4299	4809	8,209	54,469	38,584

High-resolution salinity maps were generated using Inverse Distance Weighting (IDW) interpolation of laboratory-derived soil parameters within ArcMap software. These spatial models revealed that the central zone of the study area exhibited the highest degree of salinization (Fig. 9).

Table 7. ICP-MS results – cations (g kg^{-1})

N	Na	Mg	Al	P	K	Ca
1	2.48	1.59	1.90	1.04	11.03	7.99
2	3.04	2.57	3.66	0.75	10.23	9.97
3	2.02	1.19	1.07	0.92	9.73	6.51
4	2.34	1.58	1.53	0.63	8.25	7.24
5	3.52	2.48	2.96	0.74	9.33	9.89
6	7.21	7.32	10.43	0.75	9.19	19.66

To avoid misclassification, non-agricultural features (e.g., water bodies, ponds) were excluded using a masking technique. The interpolated salinity distribution clearly shows that the central zone of the study area remains the most severely affected. This pattern corresponds with the high-density salt crusts observed in satellite imagery.

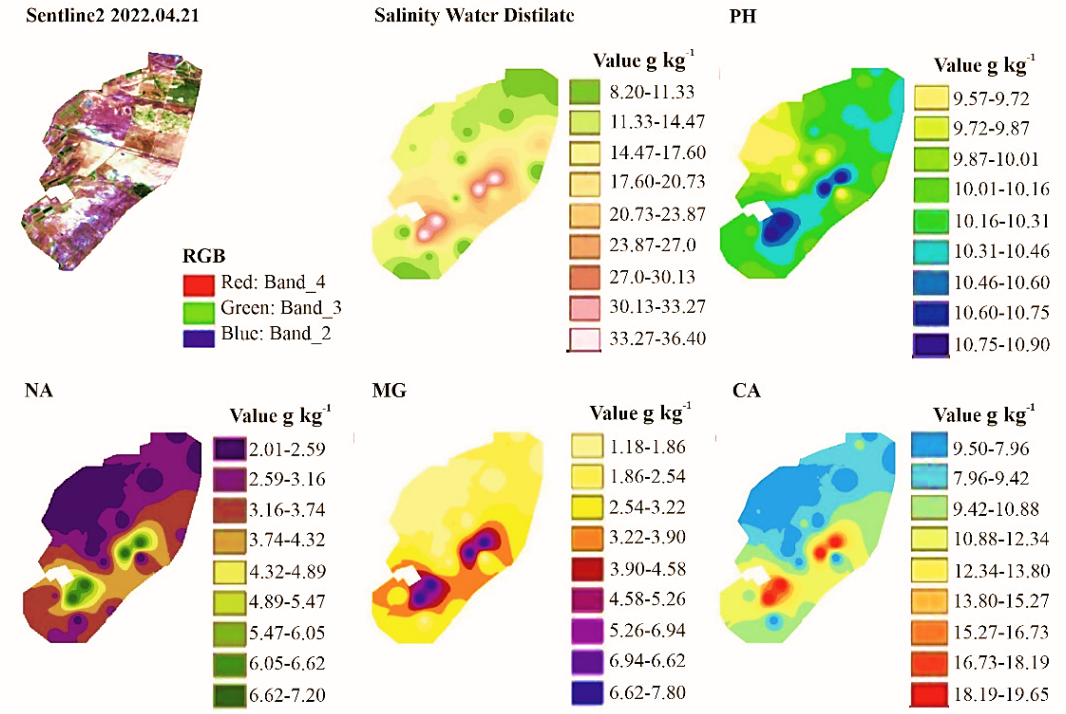

Figure 9. Interpolated salinity map (based on lab data).

Zonal statistics and accuracy assessment

Comparison of classified vector layers with the interpolation raster showed general consistency across salinity classes (severe, moderate, halophyte) regarding minimum and average values. Notable findings include:

- Minimum salinity (all classes): ~8.2 g kg^{-1}
- Maximum salinity: 36.4 g kg^{-1} in severely saline areas
- Average salinity: 15.52 g kg^{-1} (severe), 16.53 g kg^{-1} (moderate), 16.3 g kg^{-1} (halophyte)
- Na content peaks: up to 6.5 g kg^{-1} in halophyte zones; ~7.2 g kg^{-1} in others.

Interestingly, despite their bright surface crusts, the most visibly saline zones showed the lowest average water-extract salinity values.

Temporal mismatch limitation

A minor limitation stems from the temporal discrepancy between datasets. Field sampling was conducted in April 2022, whereas the classified satellite imagery is based on 2020 data. Cloud cover and low vegetation activity during spring 2022 limited satellite usability. Sentinel-2 imagery from April 21, 2022, revealed notable land-use changes, including:

- 135 ha of salinized land reclaimed:
  - ✓ 75 ha in 2021
  - ✓ 60 ha in 2022 (Fig. 10).

Agricultural interventions - particularly tillage near the railroad-adjacent zones - have altered the distribution of saline vegetation by 2022.

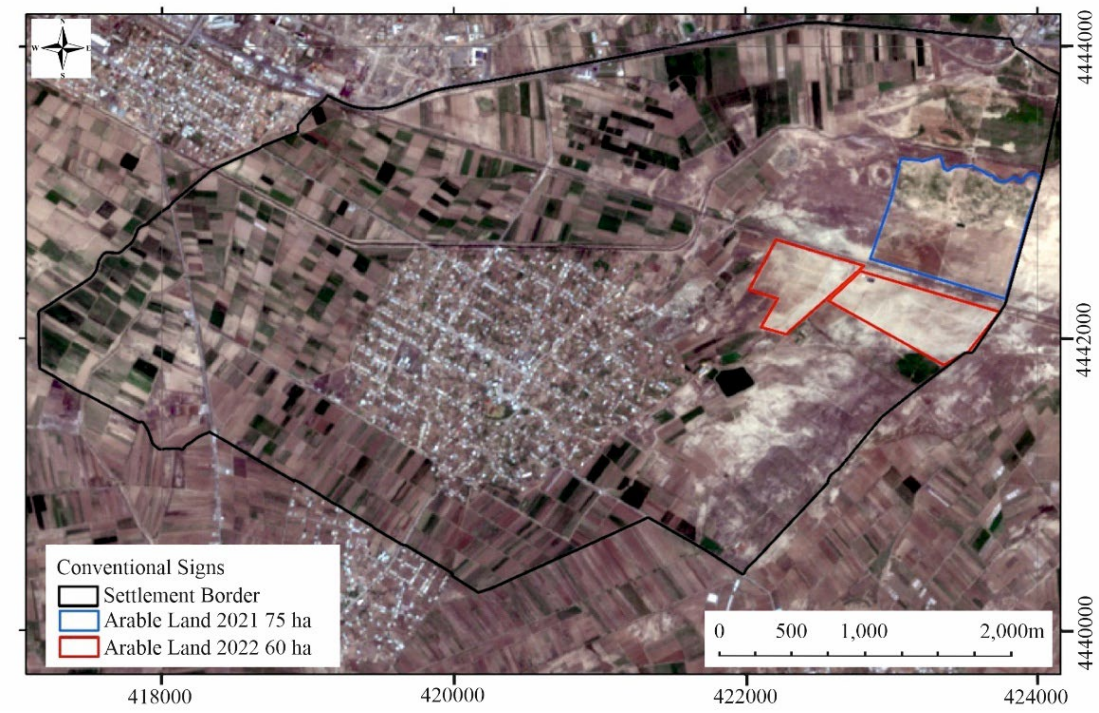

Figure 10. Sentinel-2 classification map showing reclaimed lands (April 2022).

CONCLUSION

This study demonstrates that remote sensing technologies, when integrated with GIS tools and field-based soil sampling, offer a reliable and efficient methodology for assessing and monitoring soil salinization dynamics. The use of multi-year satellite imagery, combined with vegetation and salinity indices, enabled the accurate identification and spatial classification of saline-alkaline soils in the Mrgashat settlement of the Armavir region.

Field and laboratory analyses confirmed the presence of strongly to very strongly saline soils. Water-soluble salt concentrations ranged from 8.2 to 36.4 g L^{-1}, and electrical conductivity (EC) values varied between 18.18 and 67.68 mS cm^{-1} – well above agronomic thresholds (2–16 mS cm^{-1}). Soils also exhibited high alkalinity, with pH values from 9.57 to 10.39, characteristic of soda-type saline-alkaline conditions.

Remote sensing–based land cover classification revealed a progressive increase in salinized areas over a 20-year period. In 2000, 532 hectares were affected, including:

- 244 ha with halophytic vegetation
- 208 ha of moderately saline soils
- 80 ha of highly saline soils

By 2020, the affected area had increased to 586 hectares, including:

- 195 ha with halophytic vegetation
- 293 ha of moderately saline soils
- 98 ha of highly saline soils.

This represents a net increase of 54 hectares (10.1%), with a notable expansion of moderately saline zones, indicating intensification of salinization processes.

These findings underscore the importance of integrated remote sensing and ground-truthing approaches for effective monitoring of soil degradation. Such methods are crucial for supporting sustainable land management and guiding reclamation efforts in arid and semi-arid agricultural regions.

ACKNOWLEDGEMENTS. The authors express their sincere gratitude to the staff of the Scientific Center of Soil Science, Agrochemistry and Melioration named after H. Petrosyan, Center for Agricultural Research and Certification SNCO, and the National Hydrometeorological Service of Armenia for providing technical assistance and essential data during the study.

REFERENCES

Abbas, A. & Khan, S. 2007. Using Remote Sensing Techniques for Appraisal of Irrigated Soil Salinity. In: L. Oxley and D. Kulasiri, (Eds.), *International Congress on Modelling and Simulation (MODSIM), Modelling and Simulation Society of Australia and New Zealand, Brighton,* 2632–2638. https://www.researchgate.net/publication/237421639

Abreu, A.L., Ferraz, G.A.S., Morais, R., Bento, N.L., Conti, L., Bambi, G. & Ferraz, P.F.P. 2024. Use of geostatistical analyses for wheat production areas through the variables NDVI, surface temperature, and yield. *Agronomy Research* **22**(S1), 329–345. doi: 10.15159/AR.24.021

Alhammadi, M.S. & Glenn, E.P. 2008. Detecting date palm trees' health and vegetation greenness change on the eastern coast of the United Arab Emirates using SAVI. *International Journal of Remote Sensing* **29**(6), 1745–1765. doi: 10.1080/01431160701395197

Baldina, E.A. & Nikolaev, D.S. 2024. Thermal Remote Sensing of Vegetation in Research and Education. *In: Proceedings, 9th Int. Conf. on Cartography and GIS. Nessebar, Bulgaria,* 190–199. https://iccgis2024.cartography-gis.com/papers/9ICCGIS-Proceedings_Paper%20(21).pdf

Bannari, A.M., Guedona, El-Hartib, A., Cherkaouic, F.Z. & El-Ghmari, A. 2008. Characterization of Slightly and Moderately Saline and Sodic Soils in Irrigated Agricultural Land using Simulated Data of an Advanced Land Imaging (EO-1) Sensor. *Communications in Soil Science and Plant Analysis* **39**(19–20), 2795–2811. doi: h10.1080/00103620802432717

Burke, M., Driscoll, A., Lobell, D.B. & Ermon, S. 2021. Using satellite imagery to understand and promote sustainable development. *Science* **371**(6535), 987–992. doi: 10.1126/science.abe8628

Douaoui, E.K., Nicolasb, H. & Walter, C. 2006. Detecting Salinity Hazards within a Semiarid Context by Means of Combining Soil and Remote-Sensing Data. *Geoderma* **134**(1–2), 217–230. doi: 10.1016/j.geoderma.2005.10.009

Dwivedi, R.S., Kothapalli, R.V. & Singh, A.N. 2008. Generation of Farm-level Information on Salt-affected Soils using IKONOS-II Multispectral Data. In: Metternicht, G., Zinck, J.A. (Eds.), *Remote Sensing of Soil Salinization: Impact on Land Management.* CRC Press, Taylor and Francis, New York, pp. 73–89. doi: 10.1201/9781420065039.ch5

Eldeiry, A.A & Garcia, L.A. 2008. Detecting Soil Salinity in Alfalfa Fields Using Spatial Modeling and Remote Sensing. *Soil Science Society of America Journal* **72**(1), 201–211. doi: 10.2136/sssaj2007.0013

Elnaggar, A. & Noller, J.S. 2009. Application of RemoteSensing Data and Decision-Tree Analysis to Mapping Salt-Affected Soils over Large Areas. *Remote Sensing* **2**(1), 151–165. http://dx.doi.org/10.3390/rs2010151

FAO (Food and Agriculture Organization of the United Nation). 2005. Global network on integrated soil management for sustainable use of salt-affected soils. *FAO Land and Plant Nutrition Management Service*, Rome. *http://www.fao.org/ag/agl/agll/spush*

FAO (Food and Agriculture Organization of the United Nation). 2018. *Handbook for saline soil management, Eurasian Soil Partnership Implementation Plan* **1**. Rome, 143 pp. *https://www.fao.org/documents/card/ru/c/i7318r/*

Gao, B.C. 1996. NDWI - A normalized difference water index for remote sensing of vegetation liquid water from space. *Remote Sensing of Environment* **58**(358), 257–266. doi: 10.1016/S0034-4257(96)00067-3

Hayrapetyan, E.M. 2000. *Soil Science. Yerevan*, 456 pp. (in Armenian).

Howari, F. 2003. The Use of Remote Sensing Data to Extract Information from Agricultural Land with Emphasis on Soil Salinity. *Australian Journal of Soil Research* **41**(7), 1243–1253. doi: 10.1071/SR03033

Howari, F.M., Goodell, P.C. & Miyamoto, S. 2002 Spectral properties of salt crusts formed on saline soils. *Journal of Environmental Quality* **31**, 1453–1461. doi: 10.2134/jeq2002.1453

Huete, R. 1988. A Soil-Adjusted Vegetation Index (SAVI). *Remote Sensing of Environment* **25**(3), 295–309. http://dx.doi.org/10.1016/0034-4257(88)90106-X

Jose Manuel Calderon Pincay, & Maria Fernanda Pincay Cantos. 2024 Analysis of Soil Salinization as an Environmental Issue in Latin America. *J. Ecol. Eng*. **25**(1), 146–152. doi: 10.12911/22998993/174378

Katawatin, R. & Kotrapat, W. 2005. Use of LANDSAT-7 ETM+ with Ancillary Data for Soil Salinity Mapping in Northeast Thailand. *Third International Conference on Experimental Mechanics and Third Conference of the Asian Committee on Experimental Mechanics* **5852**, 708–716. doi: 10.1117/12.621889

Khan, N.M., Rastoskuev, V.V., Sato, Y. & Shiozawa, S. 2005. Assessment of Hydrosaline Land Degradation by Using a Simple Approach of Remote Sensing Indicators. *Agricultural Water Management* **77**(1), 96–109. doi: 10.1016/j.agwat.2004.09.038

Khojoyan, A.A. 2013. *Improvement of the Reclamation Condition of Salinized and Alkalized Soils of the Ararat Plain Using Physical and Chemical Methods*. PhD Thesis, Yerevan, Agriculture 72 Bulletin, 2017/**3,** 26 pp. (in Armenian).

Koohafkan, P. & Stewart, B.A. 2008. Water and Cereals in Drylands. *The Food and Agriculture Organization of the United Nations and Earthscan*, London and Sterling, VA. *https://www.fao.org/4/i0372e/i0372e.pdf*

Matinfar, H.R., Alavi Panah, S.K., Zand, F. & Khodaei, K. 2013. Detection of Soil Salinity Changes and Mapping Land Cover Types Based upon Remotely Sensed Data. *Arabian Journal of Geosciences* **6**(3), 913–919. doi: 10.1007/s12517-011-0384-6

McFarlane, D.J., George, R.J. & Caccetta, P.A. 2004. The extent and potential area of salt-affected land in Western Australia are estimated using remote sensing and digital terrain models. *Proc of 1st National Salinity Engineering Conference 9–12 November 2004 Perth, Western Australia.* 6 pp. *http://hdl.handle.net/102.100.100/184361?index=1*

McFeeters, S.K. 1996. The Use of the Normalized Difference Water Index (NDWI) in the Delineation of Open Water Features. *International Journal of Remote Sensing* **17**, 1425–1432. doi: 10.1080/01431169608948714

Melkonyan, K.G., Ghazaryan, H.Gh. & Manukyan, R.R. 2004. Current Ecological Condition of Agricultural Soils, Land Use Level, Improvement of the Management System, and Ways to Increase Efficiency in the Republic of Armenia, Yerevan, 53 pp. (in Armenian).

Metternicht, G. & Zinck, A. 2008. Remote Sensing of Soil Salinization: *Impact on Land Management (1st ed.). CRC Press*, 377. doi: 10.1201/9781420065039

Nguyen, K.A., Liou, Y.A., Tran, H.P., Hoang, P.P. & Nguyen, T.H. 2020. Soil salinity assessment by using the near-infrared channel and the Vegetation Soil Salinity Index derived from Landsat 8 OLI data: A case study in the Tra Vinh Province, Mekong Delta, Vietnam. *Prog. Earth Planet. Sci*. **7**(1). doi: 10.1186/s40645-019-0311-0

Periasamy, S. & Ravi, K. 2020. A novel approach to quantify soil salinity by simulating the dielectric loss of SAR in three-dimensional density space. *Remote Sensing of Environment* **251**(112059). doi: 10.1016/j.rse.2020.112059

Shoba, P. & Ramakrishnan, S. Shanmugam. 2016. Multispectral and Microwave Remote Sensing Models to Survey Soil Moisture and Salinity. Land degradation & development. *Published online in Wiley Online Library* (wileyonlinelibrary.com), pp. 1–14, doi: 10.1002/ldr.2661

Silva, S.A.S., Ferraz, G.A.S., Figueiredo, V.C., Volpato, M.M.L., Machado, M.L., Silva, V.A., Matos, C.S.M., Conti, L.& Bambi, G. 2024. Spatial variability of chlorophyll and NDVI obtained by different sensors in an experimental coffee field. *Agronomy Research* **22**(S1), 554–570, doi: /10.15159/AR.24.037

Smanov, Z.M., Laiskhanov, S.U., Poshanov, M.N., Abikbayev, Y.R., Duisekov, S.N. & Tulegenov, Y.A. 2023. Mapping of Cornfield Soil Salinity in Arid and Semi-Arid Regions. *Journal of Ecological Engineering* **24**(1), 146–158. doi: 10.12911/22998993/155952

Tong, R., Ma, C., Lou, C., Yuan, W., Zhu, N., Wang, G.G. & Wu, T. 2023. Leaf nitrogen and phosphorus stoichiometry of the halophytes across China. *Front. Plant Sci*. **14**(1276699). doi: 10.3389/fpls.2023.1276699

Tucker, C.J. 1979. Red and Photographic Infrared Linear Combinations for Monitoring Vegetation. *Remote Sensing of Environment* **8**, 127–150. doi: 10.1016/0034-4257(79)90013-0

Wang, F., Yang, S.T., Wei, Y., Qian, Sh. & Jianli, D. 2021. Characterizing soil salinity at multiple depth using electromagnetic induction and remote sensing data with random forests: A case study in Tarim River Basin of southern Xinjiang, China. *Science of the Total Environment* **754**(142030). doi: 10.1016/j.scitotenv.2020.142030

Wilson, E.H. & Sader, S.A. 2002. Detection of forest harvest type using multiple dates of Landsat TM imagery: *Remote Sensing of Environment (Remote Sens. Environ.)* **80**(3), 385–396. doi: 10.1016/S0034-4257(01)00318-2

Xiang, Y., Jiaqiang, L. & Xin, G. 2022. An over review of desertification in Xinjiang, Northwest China. *Journal of Arid Land* **14**(11), 1181–1195. doi: 10.1007/s40333-022-0077-x

Yeghiazaryan, A.G. 2017. Trends in Soil Salinization Development and Assessment Results Based on the Example of the Armavir Region. *Bulletin of the National University of Architecture and Construction of Armenia*. Yerevan, **3**(56), 65–72 (in Armenian).

Yeghiazaryan, G.M. & Yeghiazaryan, A.G. 2018. On the Issue of Digital Mapping of Salinized Soils Using RS Methods in a GIS Environment. Contemporary Issues of Geography and Geology Dedicated to the 100th Anniversary of Yerevan State University, *International Conference Proceedings*, September 27–29, Yerevan (in Armenian).

Zhang, Z.C., Han, L.Y. & Pan, K.J. 2021. Sediment transport characteristics above a Gobi surface in northwestern China, and implications for aeolian environments. *Aeolian Research* **53**(100745). doi: 10.1016/j.aeolia.2021.100745